Bayesian optimal UAV trajectory planning for minimising the uncertainty of traffic density estimations

Y. Englezou[a*], S. Timotheou[a] and C. G. Panayiotou[a]

[a] KIOS Research and Innovation Center of Excellence & the Department of Electrical and Computer Engineering, University of Cyprus, Nicosia, Cyprus
englezou.yiolanda@ucy.ac.cy, timotheou.stelios@ucy.ac.cy, christosp@ucy.ac.cy
* Corresponding author

Extended abstract submitted for presentation at the Conference in Emerging Technologies in Transportation Systems (TRC-30)
September 02-03, 2024, Crete, Greece

August 9, 2024

Keywords: Gaussian process model, UAV flight path planning, traffic state estimation, uncertainty quantification, uncertainty propagation.

1 INTRODUCTION

Unmanned Aerial Vehicles (UAVs) have gained significant attention towards overcoming several limitations for traffic monitoring purposes that may arise with the use of conventional sensing technologies (Brahimi *et al.*, 2020). They offer several key advantages in monitoring traffic networks, due to their ability to fly between areas at high altitudes and collect high-quality spatiotemporal traffic-related data with no installation costs (Barmpounakis & Geroliminis, 2020). Despite the many advantages that UAVs can offer, their applicability has so far been limited to occasional surveillance of road networks through the provision of live video feeds to traffic operators or recording of videos for offline processing (Barmpounakis & Geroliminis, 2020) and extraction of historical traffic data (Barmpounakis & Geroliminis, 2020, Krajewski *et al.*, 2018).

One of the most challenging tasks of UAVs is path planning, which aims to determine the most efficient route of a UAV from an initial to a target point, with respect to a specific task to be optimised. To the best of our knowledge, there is no research work in the literature that has investigated the online construction of UAV trajectories with respect to minimising the uncertainty or maximising the information gained of traffic states.

In this work we propose an online probabilistic optimal UAV trajectory construction scheme, that strategically selects the next sampling points from which the UAV should obtain measurements of the traffic density, to minimise the total uncertainty of the traffic density in the time-horizon under study. We incorporate the Gaussian Process (GP) model into a Bayesian framework to accurately estimate the traffic density of specific road segments in a multi-lane highway, even when data points are sparse within the specified time-space region under study and develop a novel approach to obtain a Bayesian optimal UAV trajectory.

2 METHODOLOGY

2.1 Problem Formulation

Assume a traffic network that is comprised by $N^E = |\mathcal{E}|$ road segments segments. Each segment consists of N^L distinct road lanes. We monitor the traffic network for a fixed time period T and denote as $\mathcal{M}^\tau \subset \mathcal{E}$ the set of monitored segments at time-point τ, while the total number of monitored segments is $N^\tau = |\mathcal{M}^\tau|$ such that $N^\tau \leq N^E$.

We consider a collection of N^U UAVs, with identical flying and sensing capabilities, are hovering above the network. The network is discretised into P UAV sampling points, represented by $\mathcal{S}^U = \{s_1, \ldots, s_P\}$. Each UAV achieves complete coverage of the road infrastructure by visiting all sampling points. Every UAV moves between sampling points at a constant velocity equal to v^{UAV} [m/s] such that it requires $T^U_{ss'} = d_{ss'}/v^{UAV}$ [s] to travel from sampling point s to s', with $s, s' \in \mathcal{S}^U$. Here, $d_{ss'}$ represents the distance between these two sampling points.

At different sampling points, UAVs can observe specific subsets of the network, such that multiple UAVs observe potentially overlapping subsets of time-space region $\mathcal{A}$. Consolidating these time-space subsets from different UAVs yields the following measurements:

- The *density* of road segment i: $\boldsymbol{\rho}_i = [\rho_{i,1}, \ldots, \rho_{i,L_i}]^{\mathrm{T}}$ [veh/km].
- Time-window indices associated with density measurements: $\boldsymbol{\tau}_i = [\tau_{i,1}, \ldots, \tau_{i,L_i}]^{\mathrm{T}}$ [s].

Above, $\rho_{i,l}$ is the lth measurement obtained from road segment i, $\tau_{i,l} = j'$ indicates that the lth measurement corresponds to time-window $\mathcal{T}_{j'}$ and L_i is the total number of measurements in the specific road segment. The absence of index $\hat{j}$ in $\boldsymbol{\tau}_i$ indicates that no UAV has observed any part of road segment i over time-window $\mathcal{T}_{\hat{j}}$.

2.2 Solution Approach

2.2.1 Gaussian process model

Given data in the format of $(\boldsymbol{\rho}, \mathbf{Z})$, where $\mathbf{Z} = \{\mathbf{z}_{i,\tau} | i = 1, \ldots, N^E, \tau = 1, \ldots, L_i\}$ are the time-space inputs and $\boldsymbol{\rho} = \{\rho_{i,\tau} = \rho_i(\mathbf{z}_{i,\tau}) | i = 1, \ldots, N^E, \tau = 1, \ldots, L_i\}$ is the traffic density obtained at irregularly spaced sampling time-points denoted by $\boldsymbol{\tau}_j \in \mathcal{N}^W$, we make the assumption that $\boldsymbol{\rho}_i = f_i(\mathbf{Z}) + \boldsymbol{\varepsilon}_i$. Functions $f_i(\cdot)$ are unknown, and each $\boldsymbol{\varepsilon}_i$ signifies the measurement noise, independently drawn from a normal distribution $\boldsymbol{\varepsilon}_i \sim N(\mathbf{0}, \sigma^2_{i,\varepsilon}\mathbf{I})$. We have that $T = \sum_{i=1}^{N^E} L_i$ and matrix $\mathbf{Z} \in \mathbb{R}^{T \times N^E}$ has N^E blocks where the ith block is defined as $\mathbf{Z}_{\{i\}} = [\mathbf{z}_{i,1}, \ldots, \mathbf{z}_{i,L_i}]^{\mathrm{T}}$, which corresponds to the input set of function $f_i(\cdot)$. The vector of observations $\boldsymbol{\rho}$ has also N^E components such that $\boldsymbol{\rho}_i = [\rho_{i,1}, \ldots, \rho_{i,L_i}]^{\mathrm{T}}$, which corresponds to the observations of $f_i(\cdot)$ at input $\mathbf{Z}_{\{i\}}$. Our aim is to approximate each segment's output simultaneously in order to account for correlations across different road segments.

An important aspect of the GP model involves estimating the traffic density, denoted as $\tilde{\boldsymbol{\rho}}$, at an unobserved time-space point $\tilde{\mathbf{Z}}$. By employing standard results, we obtain the subsequent conditional posterior distribution $\tilde{\boldsymbol{\rho}} \mid \boldsymbol{\rho}, \sigma^2, \gamma, \nu^2 \sim \mathrm{N}\left(\mu(\tilde{\mathbf{Z}}), s^2(\tilde{\mathbf{Z}})\right)$, where

$$\mu(\tilde{\mathbf{Z}}) = \mathbf{C}(\tilde{\mathbf{Z}})^{\mathrm{T}}\boldsymbol{\Sigma}^{-1}\boldsymbol{\rho}, \quad s^2(\tilde{\mathbf{Z}}) = \sigma^2[\tilde{\boldsymbol{\Sigma}} - \mathbf{C}(\tilde{\mathbf{Z}})^{\mathrm{T}}\boldsymbol{\Sigma}^{-1}\mathbf{C}(\tilde{\mathbf{Z}})]. \tag{2}$$

Above, $\mathbf{C}(\tilde{\mathbf{Z}}) = K(\tilde{\mathbf{Z}}, \mathbf{Z}; \boldsymbol{\gamma}) = [k_{11}(\tilde{\mathbf{Z}}, \mathbf{Z}; \boldsymbol{\gamma}), \ldots, k_{1N^E}(\tilde{\mathbf{Z}}, \mathbf{Z}; \boldsymbol{\gamma})]^{\mathrm{T}}$ represents the block matrix of correlations between the traffic density at each $\mathbf{Z}$ and the traffic density at the new time-space point $\tilde{\mathbf{Z}}$. In a similar manner, $\tilde{\boldsymbol{\Sigma}} = K(\tilde{\mathbf{Z}}, \tilde{\mathbf{Z}}; \boldsymbol{\gamma})$. (1)

2.2.2 Bayesian inference

Prior distributions are specified for all unknown parameters. The joint prior distribution assumed in this work is $\pi(\sigma^2, \boldsymbol{\gamma}, \nu^2) = \pi(\sigma^2)\pi(\boldsymbol{\gamma})\pi(\nu^2)$ (Rasmussen & Williams, 2006). By applying Bayes' rule we can compute the posterior density of σ^2, $\boldsymbol{\gamma}$ and ν^2 denoted as $\pi(\sigma^2, \boldsymbol{\gamma}, \nu^2 | \boldsymbol{\rho}) \propto \pi(\sigma^2)\pi(\boldsymbol{\gamma})\pi(\nu^2)\pi(\boldsymbol{\rho} | \sigma^2, \boldsymbol{\gamma}, \nu^2)$. To derive the posterior predictive distribution for $\tilde{\boldsymbol{\rho}}$ at $\tilde{\mathbf{Z}}$, it is necessary to integrate out all unknown parameters by considering their marginal posterior distributions. We use the conditional posterior predictive distribution $\tilde{\boldsymbol{\rho}} \mid \boldsymbol{\rho}, \sigma^2, \boldsymbol{\gamma}, \nu^2 \sim \mathrm{N}\left(\mu(\tilde{\mathbf{Z}}), s^2(\tilde{\mathbf{Z}})\right)$, where $\mu(\tilde{\mathbf{Z}})$ and $s^2(\tilde{\mathbf{Z}})$ are given through Equations (2), and the posterior distribution $\pi(\sigma^2, \boldsymbol{\gamma}, \nu^2 | \boldsymbol{\rho})$ as shown above. Hence, the unconditional posterior predictive distribution, is

$$\pi(\tilde{\boldsymbol{\rho}} \mid \boldsymbol{\rho}) = \int_{\sigma^2} \int_{\Gamma} \int_{\nu^2} \pi(\tilde{\boldsymbol{\rho}} \mid \boldsymbol{\rho}, \sigma^2, \boldsymbol{\gamma}, \nu^2)\pi(\sigma^2, \boldsymbol{\gamma}, \nu^2 \mid \boldsymbol{\rho}) d\sigma^2 \, d\boldsymbol{\gamma} \, d\nu^2. \tag{3}$$

2.2.3 Bayesian optimal UAV trajectory construction scheme

We define a UAV trajectory as a sequence denoted by $\zeta = [s_{b_1}, s_{b_2}, \ldots, \mathbf{s}_{b_n}]$, comprising n points, where $\{b_1, \ldots, b_n\}$ takes values from the set of UAV sampling points $\mathcal{S}^U$. A n-size optimal UAV trajectory $\zeta^\star$ is defined by comparison with the set $\mathcal{S}$ of all possible trajectories of size n with respect to a specific criterion. A Bayesian optimal UAV trajectory $\zeta^\star$ maximises the expected utility $U(\zeta) = \mathbb{E}[u(\zeta, \boldsymbol{\theta}, \boldsymbol{\rho})]$, where the expectation is with respect to the future data $\tilde{\boldsymbol{\rho}}$ and parameters $\boldsymbol{\theta} = [\sigma^2, \boldsymbol{\gamma}, \nu^2]^{\mathrm{T}} \in \Theta$. An appropriate utility $u(\cdot)$ is the Shannon information gain between the prior and the posterior predictive distribution (Shannon, 1948). The maximisation of the expected Shannon information gain for $\tilde{\boldsymbol{\rho}}$ is equivalent to maximisation of $U(\zeta) = \int\int \log \pi(\tilde{\boldsymbol{\rho}} | \boldsymbol{\rho}, \zeta)\pi(\tilde{\boldsymbol{\rho}}, \boldsymbol{\rho} | \zeta) d\tilde{\boldsymbol{\rho}} d\boldsymbol{\rho}$, see Verdinelli *et al.* (1993), where $\pi(\tilde{\boldsymbol{\rho}} | \boldsymbol{\rho}, \zeta)$ is the posterior predictive density given in (3). The intuition behind the chosen expected utility is to find the

	Bayesian optimal UAV trajectory			Cyclical trajectory		
	95% prob. bounds	**MAPE (%)**	**MAPE SD (%)**	**95% prob. bounds**	**MAPE (%)**	**MAPE SD (%)**
Time-point 149	119.66	3.91	0.59	212.98	9.56	1.84
Time point 201	33.94	4.19	0.39	64.32	6.24	0.44
Time-point 301	42.76	3.53	0.17	95.13	5.41	0.21
Time-point 431	53.77	3.44	0.25	55.24	3.85	0.84
Total time-horizon	13.98	0.65	0.05	41.91	1.92	0.19

Table 1 – *Average 95% probability bounds, average MAPE and MAPE standard deviation (SD) of all road segments for different time-points and the total time-horizon under study.*

Bayesian optimal UAV trajectory than maximises the information gain about the traffic density at unobserved time-space points, or equivalently, that minimises the uncertainty regarding the traffic density at these points. Hence, we aim to solve the following optimisation problem

$$\zeta^{\star} \in \arg\max_{\zeta \in \mathcal{Z}} U(\zeta). \tag{4}$$

3 RESULTS

To assess the effectiveness of the proposed methodology, we conduct a simulation study using a specific segment of the M25 motorway in London, England. We operate under the constraint of having only one UAV available for traffic density measurements and define $S^U = 6$ UAV sampling points placed to cover all road segments comprehensively. The scenario under examination involves a 1.5-hour traffic simulation, initially depicting free-flow traffic conditions. However, during this period, an accident occurs resulting some segments to enter the congested regime.

We compare the estimation performance of the Bayesian optimal UAV trajectory against a basic cyclical trajectory. We calculate the average 95% probability bounds of the posterior predictive distribution, $\pi(\tilde{\boldsymbol{\rho}}|\boldsymbol{\rho})$, of all road segments for the next five moves of the UAV, as well as the average Mean Absolute Percentage Error (MAPE) of the estimated density at unobserved time-space points against the 'true' traffic density, along with the standard deviation (SD) of the MAPE to show the consistency of estimation across different road segments. The MAPE is given by MAPE $= 1/S \sum_{s=1}^{S}[(|\boldsymbol{\rho}_s^{true} - \hat{\boldsymbol{\rho}}_s|)/\boldsymbol{\rho}_s^{true}]100\%$, where $\boldsymbol{\rho}^{\text{true}}$ is the 'true' traffic density and $\hat{\boldsymbol{\rho}}$ the estimated traffic density at the S unobserved time-space points.

Table 1 presents the estimation performance of the Bayesian optimal UAV trajectory compared to the basic cyclical trajectory. We specifically examine selected time-points spanning from congested to free-flow conditions within the total study time-horizon to observe the variation in the 95% probability bounds and MAPE. Additionally, we provide these metrics for the entire time-horizon under study. At time-point 149, where the transitioning from free-flow to congested conditions has initiated, both trajectories exhibit their highest probability bounds, while at time-point 431, during free-flow conditions, both approaches yield very similar results. Notably, the probability bounds obtained using the Bayesian optimal UAV trajectory are 50% smaller than those obtained from the cyclical trajectory. The Bayesian optimal UAV trajectory improves the probability bounds by up to 70% compared to the cyclical trajectory.

To provide a deeper understanding of how the Bayesian optimal UAV trajectory is constructed considering the uncertainty of traffic density at various time-space points, we present heatmaps depicting this uncertainty at the specific time-points selected in the previous results for the different road segments of the network. These heatmaps are placed alongside with the Bayesian optimal UAV trajectory, allowing for comparison with heatmaps depicting the uncertainty obtained for the cyclical trajectory at the same time-points.

In Figure 1, the top row displays plots corresponding to the Bayesian optimal UAV trajectory, while the bottom row corresponds to the cyclical UAV trajectory. Dashed lines in all plots correspond to the UAV trajectory up to the indicated time-point, while uncertainty in traffic density estimations is depicted from the start of the study's time-horizon up to the specified time-point. Additionally, uncertainty for the prediction window duration, represented by the next $m = 5$ moves of the UAV, is included. Across all plots, the highest uncertainty for the next five moves is consistently observed in road segments 1 and 2 (congested segments). The Bayesian optimal UAV trajectory strategically selects sampling points associated with these segments to minimize resulting uncertainty. Conversely, for the cyclical UAV trajectory fails to incorporate this information, resulting in slower reduction of uncertainty regarding traffic density and higher average 95% probability bounds, as also demonstrated in Table 1.

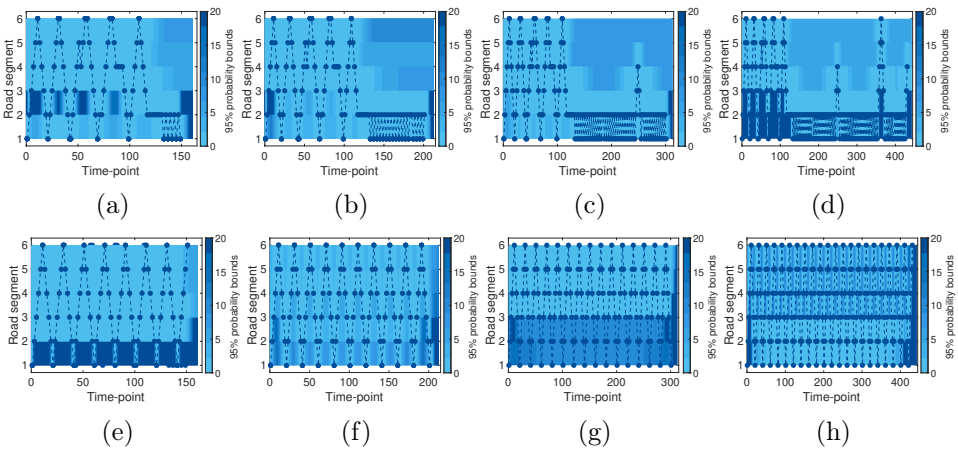

Figure 1 – *Heatmaps of the 95% probability bounds of the estimated traffic density for each road segment alongside the Bayesian UAV trajectory for time-points (a) 149, (b) 201, (c) 301, (d) 431 and the cyclical UAV trajectory (e) 149, (f) 201, (g) 301, (h) 431.*

4 DISCUSSION

In this work we propose an online Bayesian optimal UAV trajectory construction methodology to strategically select the optimal UAV sampling points in real-time, while minimizing the overall traffic density uncertainty across time and space. The proposed approach was validated using realistic simulations of a multi-lane highway stretch. Results showed that the proposed approach yields low uncertainty traffic density estimations and compared to a simple cyclical UAV trajectory, it yields a significant reduction in uncertainty of density estimates, showcasing the efficacy of our methodology for improving traffic management and planning.

Acknowledgments. This work is supported by the European Union (i. ERC, URANUS, No. 101088124 and, ii. Horizon 2020 Teaming, KIOS CoE, No. 739551), and the Government of the Republic of Cyprus through the Deputy Ministry of Research, Innovation, and Digital Strategy. Views and opinions expressed are however those of the author(s) only and do not necessarily reflect those of the European Union or the European Research Council Executive Agency. Neither the European Union nor the granting authority can be held responsible for them.

References

Barmpounakis, E., & Geroliminis, N. 2020. On the new era of urban traffic monitoring with massive drone data: the pNEUMA large-scale field experiment. *Transportation Research Part C*, 50–71.

Barmpounakis, E. N., Vlahogianni, E. I., & Golias, J. C. 2016. Unmanned Aerial Aircraft Systems for transportation engineering: current practise and future challenges. *International Journal of Transportation Science and Technology*, **5**, 111–122.

Brahimi, M., Karatzas, S., Theuriot, J., & Christoforou, Z. 2020. Drones for traffic flow analysis of urban roundabouts. *International journal of traffic and transportation engineering*, **9**, 62–71.

Englezou, Y., Timotheou, S., & Panayiotou, C. G. 2022. Probabilistic traffic density estimation using measurements from Unmanned Aerial Vehicles. *IEEE International Conference on Unmanned Aircraft Systems*.

Gohari, A., Ahmad, A., Rahim, R., Supa'at, A. S. M., & Razak, S. Gismalla, M. 2022. Involvement of Surveillance Drones in Smart Cities: A Systematic Review. *IEEE Access*, **1**.

Krajewski, R., Bock, J., Kloeker, L., & Eckstein, L. 2018. The highD Dataset: A Drone Dataset of Naturalistic Vehicle Trajectories on German Highways for Validation of Highly Automated Driving Systems. *Proceedings of the 21st International Conference on Intelligent Transportation Systems*, 2118–2125.

Rasmussen, C. E., & Williams, C. K. I. 2006. *Gaussian Processes for Machine Learning*. Cambridge: MIT Press.

Rasmussen, S., Kalyanam, K., & Kingston, D. 2016. Field experiment of a fully autonomous multiple UAV/UGS intruder detection and monitoring system. *International Conference on Unmanned Aircraft Systems*, 1293–1302.

Shannon, C. E. 1948. A Mathematical Theory of Communication. *The Bell System Technical Journal*, **27**, 379–423.

Verdinelli, I., Polson, N., & Singpurwalla, N. 1993. *Reliability and Decision Making*. Chapman and Hall/CRC. Chap. Shannon information and Bayesian design for prediction in the accelerated life testing, pages 247–256.